Dynamical back-action at 5.5 GHz in a corrugated optomechanical beam

D. Navarro-Urrios,[1,2,a] J. Gomis-Bresco,[1] S. El-Jallal,[3,4] M. Oudich,[3,b] A. Pitanti,[2] N. Capuj,[5] A. Tredicucci,[2,6] F. Alzina,[1] A. Griol,[7] Y. Pennec,[3] B. Djafari-Rouhani,[3] A. Martínez,[7] and C. M. Sotomayor Torres[1,8]

[1]*Catalan Institute of Nanoscience and Nanotechnology, Campus UAB, Edifici ICN2, 08193 Bellaterra, Spain*
[2]*NEST, Istituto Nanoscienze – CNR and Scuola Normale Superiore, Piazza San Silvestro 12, Pisa, I-56127, Italy*
[3]*IEMN, Universite de Lille 1, Villeneuve d'Ascq, France*
[4]*PRILM, Université Moulay Ismail, Faculté des sciences, Meknès, Morocco*
[5]*Depto. Física, Universidad de la Laguna, 38206, Spain*
[6]*Dipartimento di Fisica, Universita di Pisa, Largo Pontecorvo 3, I-56127 Pisa, Italy*
[7]*Nanophotonics Technology Center, Universitat Politècnica de València, Valencia, Spain*
[8]*Catalan Institution for Research and Advanced Studies (ICREA), 08010 Barcelona, Spain*

(Received 6 October 2014; accepted 5 November 2014; published online 17 November 2014)

We report on the optomechanical properties of a breathing mechanical mode oscillating at 5.5 GHz in a 1D corrugated Si nanobeam. This mode has an experimental single-particle optomechanical coupling rate of $|g_{o,OM}|$=1.8 MHz ($|g_{o,OM}|/2\pi$= 0.3 MHz) and shows strong dynamical back-action effects at room temperature. The geometrical flexibility of the unit-cell would lend itself to further engineering of the cavity region to localize the mode within the full phononic band-gap present at 4 GHz while keeping high $g_{o,OM}$ values. This would lead to longer lifetimes at cryogenic temperatures, due to the suppression of acoustic leakage. [http://dx.doi.org/10.1063/1.4902171]

Cavity optomechanics has emerged during the last decade as one of the most rapidly growing research area in science.[1] Its characteristic feature resides in the interaction between photons confined within an optical cavity and mechanical elements, which are either inside or part of the cavity, via radiation pressure forces. Functionalities such as ultrasensitive detection of small displacements/weights or possible uses in quantum information processing are some of the appealing applications motivating the interest in this field.[2]

Optomechanical (OM) cavities in which the optical decay rate is smaller than the mechanical frequency are considered to be in the sideband resolved regime. Here, the non-adiabatic response of the optical field to the mechanical actuation imprints a net phase delay on the optical force. Within that regime, if a pumping laser is red-detuned from the optical resonance of a mechanical frequency, the optical force damps the motion, effectively cooling the mechanical mode. On the other hand, if the pumping laser is tuned to the blue side of the optical resonance, the OM cavity can be driven into the "phonon lasing" regime, where the intrinsic mechanical damping can be overcame.[3] Such compact, low-power and low-phase-noise coherent oscillators are promising as frequency references for metrology applications.[4,5]

The pioneer work of Eichenfield *et al.*[6] opened the possibility of using the OM interactions at the nanoscale on a chip platform by demonstrating the concept of OM crystals. Those are quasiperiodic structures in which light and mechanical vibrations are co-localized in order to enhance the OM coupling.[7] Thanks to these properties and to the relatively low thermal population of the confined

[a]Email address: daniel.navarrourrios@nano.cnr.it
[b]Present address: Institut Jean Lamour, Université de Lorraine, Vandoeuvre-lès-Nancy, F-54500, France

mechanical modes it has been possible to cool, by optical means, an OM crystal to its quantum ground state of motion from an environmental temperature of about 20K,[8] and observe coherent effects like optomechanically induced transparency.[9]

In this work, we present an experimental characterization of a 1D OM crystal, the unit-cell of which is a Si parallelogram containing a cylindrical hole in the middle and two symmetric stubs on the side.[10] The phononic band diagram obtained with FEM simulations is reported in FIG. 1(a), where the acoustic bands highlighted in red are the only ones with the right symmetry (even-even) to couple with the optical field via radiation pressure.[10] This cell geometry exhibits the advantageous characteristic of opening a full phononic band gap around 4 GHz, as experimentally verified in ref. 11. The corresponding photonic band structure is showed in FIG. 1(b), where the band used to create the localized optical mode studied in this work is highlighted in red. The cavity region is created between two mirror regions by decreasing the pitch, radius and stubs length in a quadratic way towards the structure center. All the results presented here correspond to a structure where the maximum geometrical reduction with respect to the mirror cells is 17% and 8 periods have been considered in the defect region. Here, we focus on the confined optical and mechanical mode presenting the highest experimental OM single-particle coupling rate ($g_{o,OM}$) within the set of studied ones (green dashed lines in FIG. 1(a) and FIG. 1(b)), which, as it will be shown later on, is $|g_{o,OM}|$=1.8 MHz ($|g_{o,OM}|/2\pi$=0.3 MHz). The deformation and electric field spatial distribution associated to those modes are showed in FIG. 1(c) and FIG. 1(d) respectively. It is worth noting that the "breathing-like" mechanical mode under consideration is placed within a pseudo-gap in terms of modes of common symmetry, i.e., it is outside the full band-gap. This implies that the analyzed mode can couple with modes with different symmetries due to symmetry breaking introduced by the fabrication process.

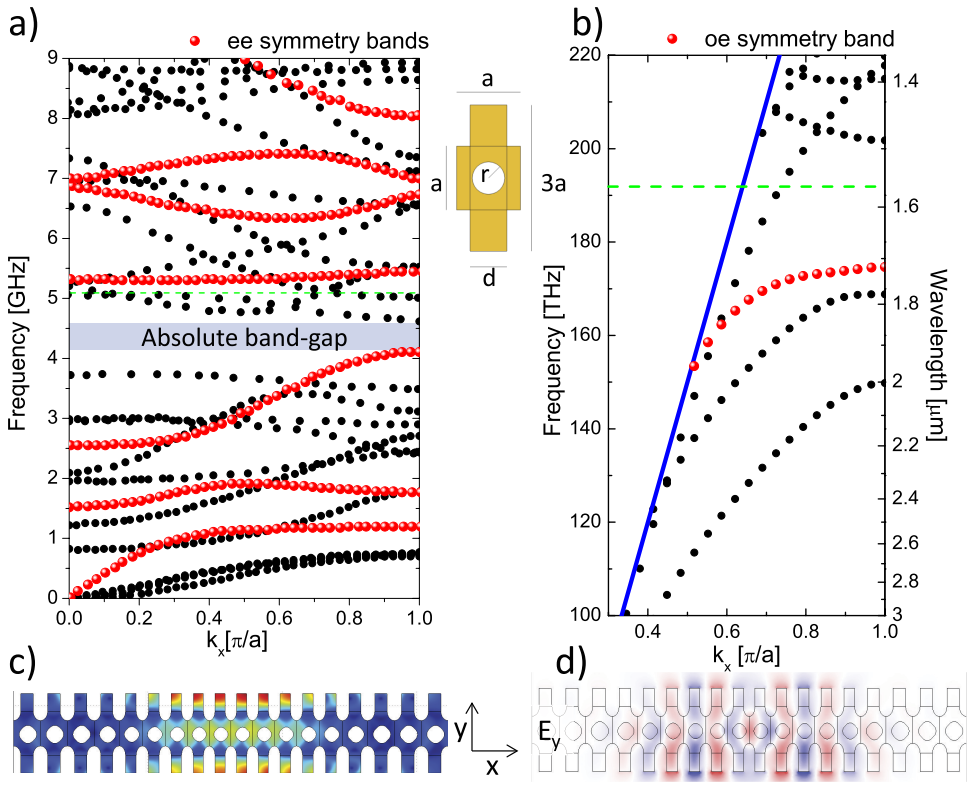

FIG. 1. Phononic and photonic band structures (panels **a)** and **b)** respectively) for wave propagation in the direction of the beam. The phononic bands with even-even symmetry and the optical bands with odd-even symmetry (see ref. 7 for more details on the symmetries definition) are highlighted in red. Both curves correspond to the fabricated unit-cell with nominal geometrical values of a=500 nm, r=150 nm, and d=250 nm (see the sketch), the Si thickness was 220 nm. The green dashed lines correspond to the localized modes discussed in this work, the deformation and electric field spatial distributions of which are illustrated in panels **c)** and **d)** respectively.

Being the latter delocalized, the coupling translates to an increase of radiation losses. However, as it was demonstrated in ref. 12, the high flexibility of the unit-cell geometry allows for large frequency tuning of the mechanical modes, thus making it possible to localize this particular one within the full band-gap while conserving a high $g_{o,OM}$,. This would lead to a significant improvement on the mechanical Q-factor at cryogenic temperatures,[11,13,14] towards efficient quantum coherent coupling between mechanical and optical modes.[9]

Single-particle OM coupling rates ($g_{o,OM}$) between optical and mechanical modes are estimated by taking into account both the photoelastic (PE) and the moving interfaces (MI) effects.[11] The PE effect is a result of the acoustic strain within bulk silicon while the MI mechanism comes from the dielectric permittivity variation at the boundaries associated with the deformation.

The calculation of the MI coupling coefficient g_{MI} is performed using the integral given by Johnson *et al.*;[15]

$$g_{MI} = -\frac{\pi\lambda_r}{c}\frac{\oint(\boldsymbol{Q}\cdot\hat{\mathbf{n}})\left(\Delta\varepsilon E_{||}^2 - \Delta\varepsilon^{-1}\boldsymbol{D}_{\perp}^2\right)dS}{\int\boldsymbol{E}\cdot\boldsymbol{D}dV}\sqrt{\hbar/2m_{eff}\Omega_m} \tag{1}$$

where **Q** is the normalized displacement (max{|**Q**|}=1), $\hat{\mathbf{n}}$ is the normal at the boundary (pointing outward), **E** is the electric field and **D** the electric displacement field. ε is the dielectric permittivity, $\Delta\varepsilon=\varepsilon_{silicon}-\varepsilon_{air}$, $\Delta\varepsilon^{-1}=\varepsilon^{-1}{}_{silicon}-\varepsilon^{-1}{}_{air}$. λ_r is the optical resonance wavelength, c is the speed of light in vacuum, $\hbar$ is the reduced Planck constant, m_{eff} is the effective mass of the mechanical mode and Ω_m is the mechanical mode eigenfrequency, so that $\sqrt{\hbar/2m_{eff}\Omega_m}$ is the zero-point motion of the resonator.

A similar result can be derived for the photo-elastic contribution:[13]

$$g_{PE} = -\frac{\pi\lambda_r}{c}\frac{\langle E|\delta\varepsilon|E\rangle}{\int\boldsymbol{E}\cdot\boldsymbol{D}dV}\sqrt{\hbar/2m_{eff}\Omega_m} \tag{2}$$

where $\delta\varepsilon_{ij}=\varepsilon_{air}\,n^4 p_{ijkl}S_{kl}$, being p_{ijkl} the photoelastic tensor components, n the refractive index of silicon, and S_{kl} the strain tensor components.

The addition of both contributions results in the overall single-particle OM coupling rate:

$$g_{o,OM} = g_{MI} + g_{PE} \tag{3}$$

For the mode under study, both contributions have the same sign, being g_{MI}=-0.49 MHz ($g_{MI}/2\pi$ =-0.08 MHz) and g_{PE}=-0.90 MHz ($g_{PE}/2\pi$=-0.14 MHz), which makes the simulated single-particle OM coupling rate $g_{o,OM}$=-1.4 MHz ($g_{o,OM}/2\pi$=-0.22 MHz).

The devices were fabricated on silicon-on-insulator (SOI) SOITEC wafers with silicon layer thickness of 220 nm (resistivity ρ ~1-10 Ω cm^{-1}, p-doping of ~10^{15} cm^{-3}) and a buried oxide layer thickness of 2 μm. The geometrical pattern was written by electron beam lithography in a 100 nm thick poly-methyl-methacrylate (PMMA) resist film and transferred into silicon through Reactive Ion Etching (RIE). Etching in BHF silicon oxide removed the buried oxide layer and released the beam structure.

The experiments were performed in a configuration suitable to characterize optical and mechanical properties of OM devices (FIG. 2(a)). A tunable infrared laser covering the spectral range between 1460-1580 nm was connected to a tapered fiber with a microloop shape, the evanescent field of which allows for the local excitation of resonant optical modes of the OM crystal. The polarization state of the light entering the tapered region was set with a polarization controller. A polarization analyzer is placed after the tapered fiber region. The OM crystal optical cavity is a bi-directional one, which can decay in both forward and backward propagating fiber modes. Only the forward channel was detected by measuring the transmitted optical power (P_{out}). The transmission spectra were collected by tuning the laser wavelength (λ_l) from short to long wavelengths. To check for the presence of a radiofrequency (RF) modulation of the transmitted signal we use an InGaAs fast photoreceiver with a bandwidth of 12 GHz. The generated RF voltage is connected to the 50 Ω input impedance of a signal analyzer with a bandwidth of 13.5 GHz. All the measurements were performed in an anti-vibration cage at atmospheric conditions of air pressure and temperature. The RF measurements were carried

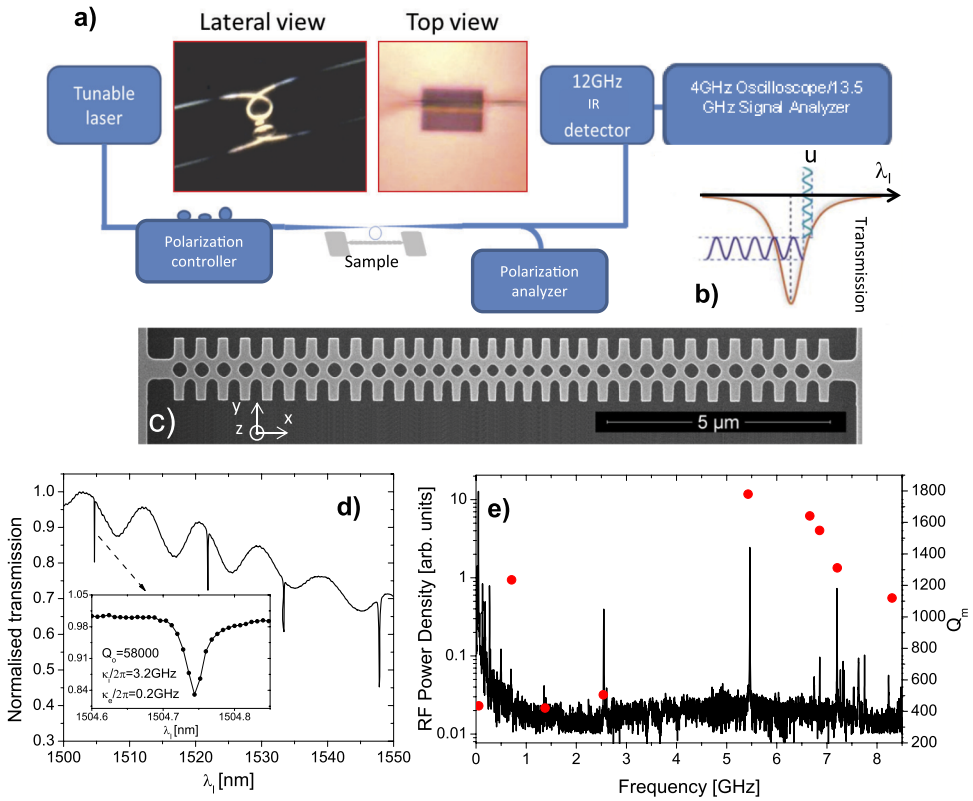

FIG. 2. **a).** Sketch of the experimental setup used to characterize the optical and mechanical properties of the OM devices. The sample size has been increased for clarity. The top left photo shows a lateral view of the real microlooped tapered fiber close to the sample, where the fiber itself can be seen reflected on the sample. The top right photo shows a top view of the tapered fiber placed parallel with the OM structure and in contact with one of the edges of the etched frame. **b)** Scheme of the transduction principle, where variations of the cavity effective length, induce fluctuations on the transmitted signal. **c)** SEM micrograph of the fabricate device. **d)** Optical transmission spectrum of the OM crystal. The inset shows a zoom of the optical mode considered in this work. **e)** RF spectrum (log scale) and mechanical Q-factor of the transduced modes.

out at a regime of input powers (P_{in}) where the typical bistability "saw-tooth" shaped transmission is observed under resonance, caused by the red-shift of λ_r due to thermo-optic (TO) nonlinearities.[16,17]

The optical spectrum extracted from the device under study (FIG. 2(c)) shows several TE polarized (electric field in the plane of the wafer) sharp resonances. The slow, overimposed modulation reflects the presence of whispering gallery modes in the microlooped tapered fiber, whose free-spectral-range decreases with the microloop radius. In the following, we focus on the first optical mode of the OM crystal cavity, corresponding to that illustrated in FIG. 1(b) and FIG.1(d). At low input powers, its spectral width is about 0.03 nm, which translates into maximum optical Q-factors ($Q_o=\lambda_r/\delta\lambda$) of 58000 (inset of FIG. 2(d)). The optical Q-factor can be also written as $Q_o=2\pi c/(\kappa\lambda_r)$, where κ=3.4 GHz is the overall decay rate of the stored optical energy resulting of the combination of the intrinsic and extrinsic decay rates (κ_i=3.2 GHz and κ_e=0.2 GHz respectively). It is worth noting that it is possible to extract κ_i and κ_e independently by measuring the transmitted power fraction, which in the case under study is $P_{out}/P_{in}=(1-\kappa_e/\kappa)^2$.[18] The intrinsic and extrinsic decay rates allows for the evaluation of the intracavity photon number, expressed as $n_o=2P_{in}(\kappa_e/(\kappa^2+\Delta^2))\lambda_r/hc$, where $\Delta=2\pi c(\lambda_l^{-1}-\lambda_r^{-1})$ is the laser detuning from the optical cavity. On resonance, the mechanical brownian motion imprints fluctuations on the optical resonance frequency around its "average" value (FIG. 2(b)).

When exciting the optical mode, a strong RF transduced signal is observed corresponding to mechanical modes distributed over a spectral range between 10 MHz and 9 GHz (FIG. 2(e)). The

mechanical quality factor ($Q_{m,i}$) spectrum at 300 K is also reported in FIG. 2(e). The maximum $Q_{m,i}$=1600 is found for the 5.5 GHz mode, which corresponds to an intrinsic mechanical damping rate $\Gamma_{m,i}$=21 MHz. The dominant damping mechanism for the modes above 5 GHz is scattering with thermal phonons. Regarding lower frequency modes, damping processes different than the latter can be dominant. It is of particular interest the case of the 2.6 GHz mode (calculated $g_{o,OM}$=1.9 MHz), which is created from k_x=0 as a result of pulling up the third even-even phononic band of FIG. 1(a).[12] The prevailing damping process is, in this case, parasitic coupling to equi-frequency waveguide modes of the same symmetry, limiting the experimental Q-factor to $Q_{m,i}$=400.

In the following, we describe the method we used to evaluate experimentally $g_{o,OM}$. We have assumed no extra losses are present in the structure under the input power conditions used to transduce the thermal motion ($P_{in,high}$), i.e., Q_o remains unaltered with respect to the low power case ($P_{in,low}$) in which thermo-optic dispersion is negligible. The optical spectra taken using $P_{in,low}$ and $P_{in,high}$ are shown in the bottom panel of FIG. 3(a) (solid and dashed curves respectively), where the experimental condition for transducing the modes is highlighted with a green circle. Under the previous assumption, and given the fact that the dynamics of the TO effect is much slower (~μs) than the mechanical oscillation (~ns), the transmitted fraction of the two curves can be directly compared to determine the laser-cavity detuning Δ. The slope of the resonance ($dP_{out}/d\lambda_l$) is then calculated in the equivalent $P_{in,low}$ point and then scaled by $P_{in,high}/P_{in,low}$. The derivative of the resonance for the $P_{in,low}$ case is plotted in the upper panel of FIG. 3(a).

A reference sinusoid signal of known amplitude (ΔP_{out}=1.24 μW) generated with an analog amplitude optical modulator is introduced to calibrate the scale of the signal analyzer (grey curve in FIG. 3(b)). This allows for an estimation of the averaged variation of P_{out} associated to the thermal motion by integrating the spectral density across the mechanical peak, providing a result that can be linked to the variance of the resonant wavelength $<\Delta\lambda_r^2>$ using the already known derivative $dP_{out}/d\lambda_l$. Finally, it can be demonstrated that $< \Delta\lambda_r^2 >= \left(\frac{2\pi c}{\lambda_r^2}\right)^2 2g_{o,OM}^2 < n_m >$,[19] where the average phonon occupation number ($<n_m>$) at 300 K is $< n_m > \approx k_B T/\hbar\Omega_m = 1143$ for the 5.5 GHz mode. This procedure yields an absolute value of the zero-point optomechanical coupling rate of $|g_{o,OM}|$=1.8 MHz ($|g_{o,OM}|/2\pi$=0.3 MHz), roughly in agreement with the calculated value ($g_{o,OM}$= -1.4 MHz).

The explicit expression for the optomechanical damping rate (Γ_{OM}) under the conditions of weak laser drive ($g_{o,OM}\sqrt{n_o}<<\kappa$) given by:

$$\Gamma_{OM}(\Omega_m) = -g_{o,OM}^2 n_o \left[\frac{\kappa}{(\Delta - \Omega_m)^2 + \kappa^2/4}\right] \quad , \tag{4}$$

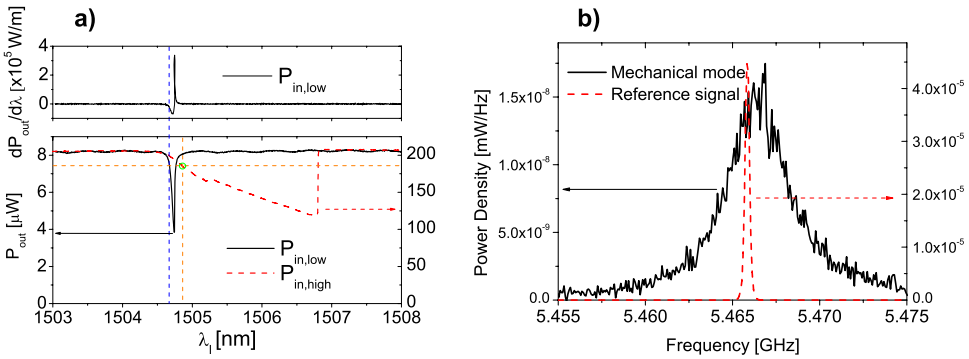

FIG. 3. **a)** Lower panel. Optical transmission around the region of the first optical resonance at low (solid curve) and high (dashed curve) P_{in}. The green circle indicates the excitation conditions for transducing the mechanical modes. The intersection between the dashed horizontal orange line and the black solid curve gives the equivalent point for the low power curve. Upper panel. The first derivative of the transmitted power under low-power conditions (black curve of the lower panel). The intersection with the vertical blue dashed line gives the slope of the resonance at the equivalent point. **b)** RF signal corresponding to the mechanical mode at 5.5 GHz (solid) and to the reference (dashed).

where we have taken into account that the mechanical mode at 5.5 GHz is within the resolved sideband approximation ($\Omega_m/\kappa \sim 2$) and that the experiment is done on the blue-side of the resonance. The overall damping rate is given by $\Gamma_m = \Gamma_{m,i} + \Gamma_{OM}$, achieving transparency when $\Gamma_{m,i} = \Gamma_{OM}$. In FIG. 4 we show the mechanically transduced peak as a function of the laser detuning Δ. The number of intracavity photons is increased from $n_o = 3\text{x}10^3$ at $\Delta = 2\pi$(8.0 GHz) (black curve) to $n_o = 5\ \text{x}10^3$ at $\Delta = 2\pi$ (5.8 GHz) (orange curve) in the set of curves. We measured an enhancement of the mechanical Q-factor up to $Q_m = 7\text{x}10^5$ consistent with an overall damping rate of $\Gamma_m = 49$ KHz, i.e., a reduction of almost three orders of magnitude with respect to the intrinsic damping rate. Interestingly, sidebands associated to lower frequency mechanical modes appear as a result of non-linearities related with the large oscillation amplitude. In fact, the side peaks of FIG. 4 correspond to flexural in-plane modes at 54 MHz and 120 MHz.[20]

A spontaneously triggered self-pulsing (SP) mechanism[20] has prevented the resonance condition of Eq. (4) from being achieved. The minimum detuning reached without inducing SP was about $\Delta = 2\pi$(5.8 GHz). Under that minimum value the SP mechanism forces the resonance frequency to oscillate across the laser wavelength with larger spectral amplitude than the resonance linewidth itself.

Summarizing, we have studied optical back-action effects on a particular mechanical mode at 5.5 GHz in a corrugated OM beam with cylindrical holes. The absolute value of the single-particle OM coupling rates was experimentally determined to be 1.8 MHz, while the absolute calculated value, taking into account the additive contributions of photoelastic and moving interfaces effects, is 1.4 MHz. Strong mechanical amplification was observed when pumping on the blue-side of the optical resonance; even if self-pulsing effects prevented the realization of the optimum relative laser-cavity detuning to maximize the anti-damping effect. As demonstrated in a previous work, the high flexibility of the unit-cell geometry enables the wide tuning of the localized modes frequency by properly engineering the cavity region. This would allow shifting this particular mode to the phononic full gap region characteristic of the corrugated unit-cell while keeping the high OM coupling rates. As a consequence, the mechanical Q-factor at cryogenic temperatures would be significantly increased. This is of key importance for quantum nonlinear optics and mechanics experiments.

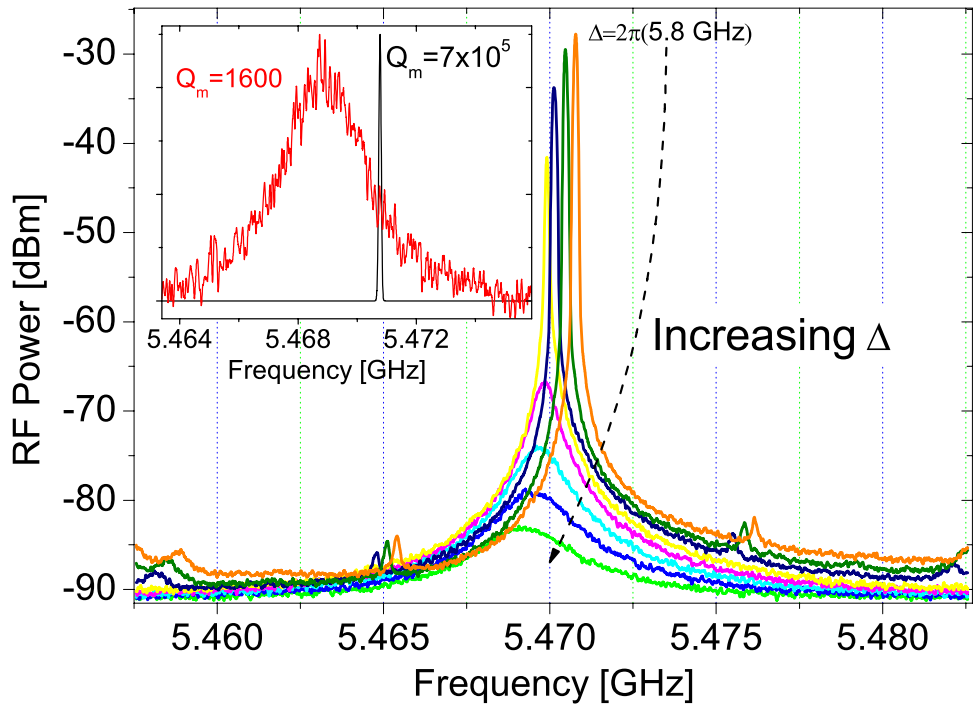

FIG. 4. Mechanical mode at 5.5GHz optically amplified through a dynamical back-action process. Different curves correspond to different cavity detuning. In the inset, the curves obtained in the extreme detuning cases of the main panel are normalized and represented in linear scale.

ACKNOWLEDGMENTS

This work was supported by the EU through the FP7 project TAILPHOX (ICT-FP7-233883) and the ERC Advanced Grant SOULMAN (ERC-FP7-321122) and the Spanish projects TAPHOR (MAT2012-31392). D.N-U and J.G-B acknowledge support in the form of postdoctoral fellowships from the Catalan (Beatriu de Pinòs) and the Spanish (Juan de la Cierva) governments, respectively.

[1] M. Aspelmeyer, T. J. kippenberg, and F. Marquardt Eds., "*Cavity Optomechanics*" (Springer, Berlin Heidelberg, 2014).
[2] M. Aspelmeyer, T. J. Kippenberg, F. Marquardt, arXiv:1303.0733 (2013).
[3] T. J. Kippenberg, H. Rokhsari, T. Carmon, A. Scherer, and K. J. Vahala, Phys. Rev. Lett. **95**, 033901 (2005).
[4] M. Hossein-Zadeh, H. Rokhsari, A. Hajimiri, and K. J. Vahala, Phys. Rev. A **74**, 023813 (2006).
[5] S. Tallur, S. Sridaran, S. A. Bhave, and T. Carmon, Frequency Control Symposium (FCS), 2010 IEEE International (IEEE, 2010), p. 268.
[6] M. Eichenfield, J. Chan, R. Camacho, K. J. Vahala, and O. Painter, Nature **462**, 78 (2009).
[7] Y. Pennec, V. Laude, N. Papanikolaou, B. Djafari-Rouhani, M. Oudich, S. El Jallal, J. C. Beugnot, J. M. Escalante, and A. Martínez, Nanophotonics to appear (2014).
[8] J. Chan, T. P. M. Alegre, A. H. Safavi-Naeini, J. T. Hill, A. Krause, S. Gröblacher, M. Aspelmeyer, and O. Painter, Nature **478**, 89 (2011).
[9] A. H. Safavi-Naeini, T. P. Mayer Alegre, J. Chan, M. Eichenfield, M. Winger, Q. Lin, J. T. Hill, D. E. Chang, and O. Painter, Nature **472**, 69–73 (2011).
[10] Y. Pennec, B. Djafari Rouhani, C. Li, J. M. Escalante, A. Martinez, S. Benchabane, V. Laude, and N. Papanikolaou, AIP Advances **1**, 041901 (2011).
[11] J. Gomis-Bresco, D. Navarro-Urrios, M. Oudich, S. El-Jallal, A. Griol, D. Puerto, E. Chavez, Y. Pennec, B. Djafari-Rouhani, F. Alzina, A. Martínez, and C. M. Sotomayor Torres, Nat. Commun. **5**, 4452 (2014).
[12] M. Oudich, S. El-Jallal, Y. Pennec, B. Djafari-Rouhani, J. Gomis-Bresco, D. Navarro-Urrios, C. M. Sotomayor Torres, A. Martínez, and A. Makhoute, Phys. Rev. B **89**, 245122 (2014).
[13] J. Chan, A. H. Safavi-Naeini, J. T. Hill, S. Meenehan, and O. Painter, Appl. Phys. Lett. **101**, 081115 (2012).
[14] A. H. Safavi-Naeini, J. T. Hill, S. Meenehan, J. Chan, S. Gröblacher, and O. Painter, Phys. Rev. Lett. **112**, 153603 (2014).
[15] S. G. Johnson, M. Ibanescu, M. A. Skorobogatiy, O. Weisberg, J. D. Joannopoulos, and Y. Fink, Phys. Rev. E **65**, 066611 (2002).
[16] D. Navarro-Urrios, J. Gomis-Bresco, N. E. Capuj, F. Alzina, A. Griol, D. Puerto, A. Martínez, and C. M. Sotomayor-Torres, J. Appl. Phys. **116**, 093506 (2014).
[17] P. E. Barclay, K. Srinivasan, and O. Painter, Opt. Express **13**, 801 (2005).
[18] J. Chan, Ph.D. thesis, California Institute of Technology, Los Angeles, 2014.
[19] M. L. Gorodetksy, A. Schliesser, G. Anetsberger, S. Deleglise, and T. J. Kippenberg, Opt. Express **18**, 23236–23246 (2010).
[20] D. Navarro-Urrios, N. E. Capuj, J. Gomis-Bresco, F. Alzina, A. Pitanti, A. Griol, and A. Martinez, C. M. Sotomayor Torres, arXiv preprint arXiv:1403.6043 (2014).